

# Quantum Criticality and Spin Liquid Phase in the Shastry-Sutherland model

Jianwei Yang,<sup>1</sup> Anders W. Sandvik,<sup>2,3,\*</sup> and Ling Wang<sup>4,†</sup>

<sup>1</sup>*Beijing Computational Science Research Center, 10 East Xibeiwang Road, Beijing 100193, China*

<sup>2</sup>*Department of Physics, Boston University, 590 Commonwealth Avenue, Boston, Massachusetts 02215, USA*

<sup>3</sup>*Beijing National Laboratory for Condensed Matter Physics and Institute of Physics, Chinese Academy of Sciences, Beijing 100190, China*

<sup>4</sup>*Department of Physics, Zhejiang University, Hangzhou 310000, China*

(Dated: May 15, 2022)

Using the density-matrix renormalization group method for the ground state and excitations of the Shastry-Sutherland spin model, we demonstrate the existence of a narrow quantum spin liquid phase between the previously known plaquette-singlet and antiferromagnetic states. Our conclusions are based on finite-size scaling of excited level crossings and order parameters. Together with previous results on candidate models for deconfined quantum criticality and spin liquid phases, our results point to a unified quantum phase diagram where the deconfined quantum-critical point separates a line of first-order transitions and a gapless spin liquid phase. The frustrated Shastry-Sutherland model is close to the critical point but slightly inside the spin liquid phase, while previously studied unfrustrated models cross the first-order line. We also argue that recent heat capacity measurements in  $\text{SrCu}_2(\text{BO}_3)_2$  show evidence of the proposed spin liquid at pressures between 2.6 and 3 GPa.

The quasi two-dimensional (2D)  $S = 1/2$  quantum magnet  $\text{SrCu}_2(\text{BO}_3)_2$  [1–3] has emerged [4–9] as the most promising material for realizing the deconfined quantum-critical point (DQCP) [10–12], where a gapped state with a spontaneously formed singlet pattern meets a gapless antiferromagnetic (AF) state in a phase transition associated with fractionalized excitations (spinons). The intralayer interactions of the Cu spins correspond to the Shastry-Sutherland (SS) model [13], with highly frustrated AF interdimer ( $J$ ) and intradimer ( $J'$ ) Heisenberg couplings. This model has three known ground states versus  $g = J/J'$ ; a dimer singlet (DS) state for small  $g$  [13], a Néel AF state for large  $g$ , and a two-fold degenerate plaquette-singlet (PS) state for  $\alpha \in [0.68, 0.77]$  [3, 6, 14, 15].

At ambient pressure  $\text{SrCu}_2(\text{BO}_3)_2$  is in the DS phase [1, 2] but it had been anticipated that the other SS phases may be reached under high pressure [16]. Recent heat capacity [7, 8], neutron scattering [4], and Raman [9] experiments indeed detected phase transitions and excitations that confirm some variant [17] of the PS phase (from 1.7 to 2.5 GPa at temperatures below 2 K) and an AF phase (between 3 and 4 GPa below 4 K). A direct PS–AF transition may then be expected at low-temperature between 2.6 and 3 GPa [18].

Here we show that the above picture is incomplete. Using the density-matrix renormalization group (DMRG) method [19], we study the ground state and low-lying excitations of the SS model. Based on the lattice size dependence of the level spectrum and order parameters, we conclude that there is a narrow gapless spin liquid (SL) phase intervening between the PS and AF phases. In light of this finding, the lack of signs of any phase transition between 2.6 and 3 GPa in the recent heat capacity measurements on  $\text{SrCu}_2(\text{BO}_3)_2$  [7, 8] opens the intriguing prospect of an SL in this material.

*DMRG calculations.*—The SS model with AF couplings  $J$  between first neighbor spins  $\langle ij \rangle$  and  $J'$  on a subset of second neighbors  $\langle ij' \rangle'$  is illustrated in Fig. 1. The Hamiltonian is [13]

$$H = J \sum_{\langle ij \rangle} \mathbf{S}_i \cdot \mathbf{S}_j + J' \sum_{\langle ij' \rangle'} \mathbf{S}_i \cdot \mathbf{S}_{j'}, \quad (1)$$

here on  $L_x \times L_y$  cylinders [20, 21] with open and periodic boundary conditions in the  $x$  and  $y$  direction, respectively, and  $L_y \equiv L = 2n$ ,  $L_x = 2L$ . In this geometry, the model has a preferred singlet pattern which minimizes the boundary energy in the PS phase; thus the two-fold degeneracy is broken and the ground state is unique, as illustrated in Fig. 1.

We have developed efficient procedures for calculating not only the ground state with full  $\text{SU}(2)$  symmetry [22, 23], but also successively generating excited states by orthogonalizing to previous states [24–26]. We have run the DMRG calculations with stringent convergence criteria for given Schmidt number  $m$  and used sufficiently large  $m$  for reliably extrapolating to discarded weight  $\epsilon_m = 0$  (illustrated in the Supplemental Material [27]) for  $L$  up to 10, 12, or 14 depending on quantity. Any remaining errors in the results are small on the scale of the graph symbols in the figures presented below.

We focus on  $g \in [0.7, 0.9]$ , which according to previous works straddles the PS and AF phases. The ground state of the system is always a singlet, and we will analyze the gaps  $\Delta(S)$  to the lowest excited singlet ( $S = 0$ ), triplet ( $S = 1$ ), and quintuplet ( $S = 2$ ). Finite-size crossings of excited levels with different spin have often been used as indicators of quantum phase transitions in spin chains [28–30], and this method was also applied to the 2D  $J$ - $Q$  [31] and  $J_1$ - $J_2$  [25, 32, 33]

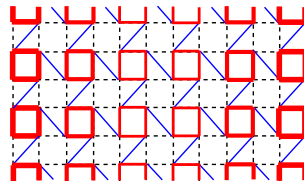


Figure 1. The SS lattice with open  $x$  and periodic  $y$  boundary conditions. The lengths  $L_x$  and  $L_y$  are both even. Nearest neighbors are coupled at strength  $J$  by Eq. (1) and the blue diagonal links represent the dimer couplings  $J'$ . The open edges break the  $\mathbb{Z}_2$  symmetry of the PS phase, thus inducing a singlet density pattern as indicated schematically by the thickness of the red lines.

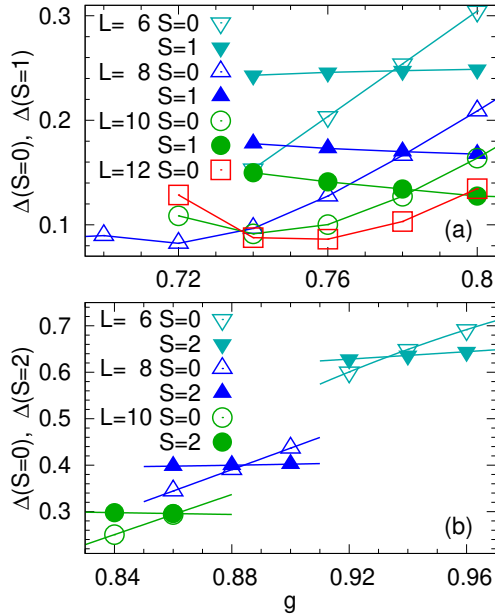


Figure 2. (a) The lowest singlet and triplet gaps vs  $g$  in the neighborhood of the expected quantum phase transition out of the PS phase. (b) The lowest singlet and quintuplet gaps for  $g$  inside the AF phase, close to its quantum phase transition.

Heisenberg models. Here we will study level crossings with the aim of detecting the transitions out of the PS phase and into the AF state, following Ref. 25 closely. We also study the PS and AF order parameters to further corroborate the quantum phases and phase transitions.

We graph singlet and triplet gaps in Fig. 2(a) and similarly singlet and quintuplet gaps in Fig. 2(b), in  $g$  windows where gap crossings are observed. In Fig. 3 we analyze the gap crossing points as well as the singlet minimum that is also observed in Fig. 2(a). Given the previous empirical observations of finite-size drifts of crossing points in 2D systems [25, 31], we graph the results versus  $1/L^2$  and find almost perfect linear behaviors in this variable. Interesting, the singlet-triplet crossings and the singlet minimum both extrapolate to a point  $g_{c1} \approx 0.79$ , while the singlet-quintuplet points scale to a higher value;  $g_{c2} \approx 0.82$ .

It was previously shown [25, 30] that the crossing point between the lowest singlet and quintuplet levels is a useful finite-size estimator for a quantum phase transition into an AF phase, given that the lowest  $S > 0$  states are Anderson quantum rotors, separated from the ground state by gaps  $\Delta_A(S) \propto S(S+1)/L^2$  (in 2D), while the singlet excited state is unrelated to the rotor tower and should be at higher energy. In fact, the singlet should correspond to the gapped amplitude (“Higgs”) mode in the AF state [6]. In contrast, in other putative phases adjacent to the AF phase (in the SS model and many other models), the  $S = 2$  state should be above the lowest  $S = 0$  excitation. Thus, we identify the extrapolated singlet-quintuplet crossing point  $g_{c2} \approx 0.82$  with a quantum phase transition into the AF state.

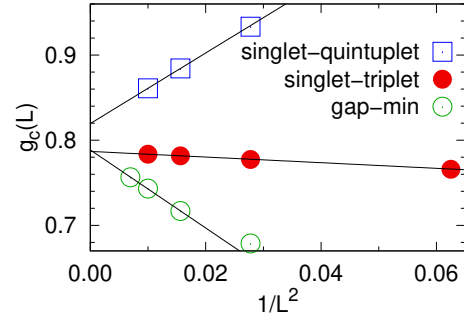


Figure 3. Locations of gap crossings and singlet minimum, with the lines showing linear-in- $1/L^2$  fits. The  $L = 4$  singlet-quintuplet point is at  $g \approx 1.1$ , falling very close to the fitted line. The extrapolated critical points are  $g_{c1} = 0.787 \pm 0.002$  and  $g_{c2} = 0.820 \pm 0.002$ .

Following the previous work on the  $J_1$ - $J_2$  model [25], we identify the extrapolated singlet-triplet crossing point  $g_{c1} \approx 0.79$  with the transition out of the PS state. The singlet minimum by itself is consistent with the PS gap vanishing at a DQCP and becoming the gapped amplitude mode in the AF phase [6]. However, an AF phase starting at  $g_{c1}$  is inconsistent with the significantly higher singlet-quintuplet crossing point  $g_{c2}$ . Below we will show additional evidence of a gapless SL phase for  $g \in (g_{c1}, g_{c2})$ .

Though the separation between the transition points  $g_{c1} \approx 0.79$  and  $g_{c2} \approx 0.82$  is small, an eventual flow toward a common point for larger systems appears unlikely, given the absence of significant corrections to the  $1/L^2$  forms in Fig. 3. The singlet-triplet and singlet-quintuplet crossings both match those previously identified in the  $J_1$ - $J_2$  Heisenberg model [25], where several studies using different numerical techniques now have reached a consensus on the existence of a gapless SL phase between a columnar dimerized phase and the AF phase [23, 25, 32–34]. A quantum field theory was very recently proposed to account for this SL phase [35]. The same level crossings were also previously found at the transition from a gapless critical state to either a dimerized state (singlet-triplet crossing) or an AF state (singlet-quintuplet crossing) in a frustrated Heisenberg chain with long-range interactions [25, 30]. In light of all these results for related models and the distinct  $g_{c1}$  and  $g_{c2}$  points identified here, a gapless SL phase in the SS model is plausible.

In Fig. 4 we analyze the size dependence of the singlet gaps for  $g$  in and close to the putative SL phase. At  $g = 0.80$ , which should be inside the SL phase, the gaps are consistent with asymptotic  $1/L$  scaling. The results for  $g = 0.78$  and  $0.82$ , close to  $g_{c1}$  and  $g_{c2}$ , respectively, also are consistent with linear scaling. Thus, our results suggest a dynamic exponent  $z = 1$  for the SL phase and its quantum phase transitions, though slightly higher  $z$  (as has been argued at the DQCP in the  $J_1$ - $J_2$  model [35]) cannot be ruled out. The finite-size singlet gap minimum [Fig. 2(a) and Fig. 3] would be explained if  $z = 1$  in the SL phase and  $z > 1$  at  $g_{c1}$ . We have triplet gaps for  $L$  up to 10 and they also are consistent with  $1/L$  scaling in the SL phase.

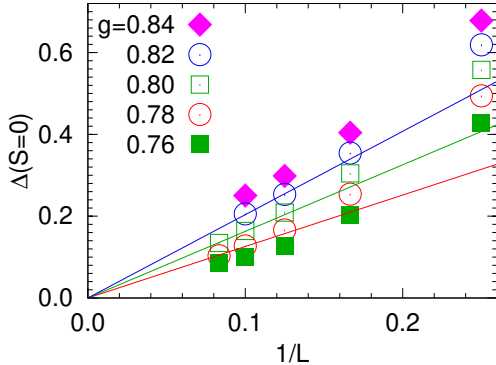


Figure 4. Singlet gaps vs inverse system size. Lines with zero intercept have been fitted to the  $g = 0.78$ ,  $0.80$ , and  $0.82$  data. At  $g = 0.78$  the system is slightly inside the PS phase, and the linear form should not apply asymptotically due to the gap (note that the  $g = 0.76$  data flatten out clearly). At  $g = 0.84$  the system is in the AF phase and the singlet represents the gapped amplitude mode.

We next study order parameters. We use the standard AF magnetization,  $m_s^2 = L^{-4} \sum_{ij} \phi_{ij} \langle \mathbf{S}_i \cdot \mathbf{S}_j \rangle$ , where  $i, j$  are sites in the central  $L \times L$  area of a  $2L \times L$  system and  $\phi_{ij} = \pm 1$  is the staggered phase. To detect PS order we define  $\mathbf{Q}_r \equiv \frac{1}{2}(\mathbf{P}_r + \mathbf{P}_r^{-1})$ , with  $\mathbf{P}_r$  a cyclic permutation operator on the four spins of a plaquette at  $r$ . Given the boundary-induced plaquette pattern (Fig. 1), we can detect the PS order as the difference of  $\langle \mathbf{Q}_r \rangle$  on two adjacent 'empty' SS plaquettes [36]. Thus, we define  $m_p = \langle \mathbf{Q}_R - \mathbf{Q}_{R'} \rangle$ , where  $R$  and  $R'$  are both close to the center of the cylinder (the landscape of  $\mathbf{Q}_r$  values is shown in the Supplemental Material [27]). Both order parameters are graphed versus  $1/L$  in Fig. 5.

Second-order polynomial extrapolations of the AF order parameter in Fig. 5 show that  $m_s^2$  vanishes for  $g \approx 0.82$ . The polynomial form is strictly appropriate only inside the AF phase, while at a critical point  $m_s^2 \propto 1/L^{1+\eta}$  should instead apply asymptotically. The  $g = 0.82$  data can indeed be almost perfectly fitted to this power law with  $\eta \approx 0.20$ , thus providing further evidence for the AF phase starting at the extrapolated singlet-quintuplet point  $g_{c2} \approx 0.82$ , significantly above the previous estimates.

As shown in the inset of Fig. 5, the PS order increases rapidly with  $L$  inside the PS phase ( $g = 0.74, 0.76, 0.78$ ), reflecting large fluctuations and no stable order in small systems even with the symmetry-breaking cylinder edges (see Supplemental Material [27]). The boundary induced PS order close to the edges also first increases with  $L$  for values of  $g$  outside the PS phase, thus causing a non-monotonic behavior which is seen clearly for  $g = 0.82$  and  $0.84$ . The central plaquettes where  $m_p$  is defined are close to the edge for small  $L$ , and only for larger  $L$  can these plaquettes reflect the behavior of a disordered bulk. At  $g = 0.80$ ,  $m_p$  for  $L = 14$  also falls below the value for  $L = 12$ , indicating that indeed  $m_p \rightarrow 0$  when  $L \rightarrow \infty$ , as it should in the SL phase.

*DQCP and unified phase diagram.*—The originally proposed DQCP scenario is generic, with the critical point typ-

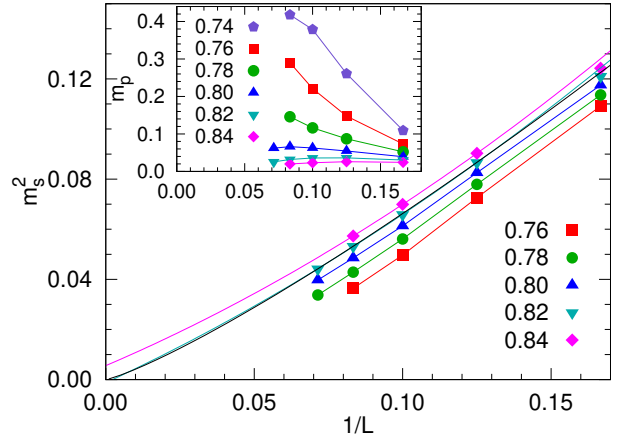


Figure 5. Squared AF order parameter vs inverse system size for several  $g$  values. The corresponding PS order parameters are shown in the inset. The curves with colors matching the  $m_s^2$  symbols for  $g = 0.82$  and  $0.84$  are second-order polynomials, while the black curve fitted to the  $g = 0.82$  data is  $\propto L^{-(1+\eta)}$  with  $\eta = 0.20$ . Fitting to the  $m_p$  data is not meaningful, but the non-monotonic behavior for  $g = 0.80-0.84$  is explained by boundary PS order outside the PS phase (Supplemental Material [27]) and  $m_p \rightarrow 0$  for  $L \rightarrow \infty$ .

ically reachable by tuning a single parameter [10]. Large-scale quantum Monte Carlo studies of several variants of  $J$ - $Q$  Hamiltonians [12] have indeed found direct transitions between the AF ground state and a four-fold degenerate columnar dimerized state [37–48]. Similar results have been obtained with related classical loop [49, 50] and dimer [51] models. In most of these models, no clear signs of discontinuities were observed, though unusual scaling violations have prompted proposals of a weak first-order transition [38, 45, 52] or other scenarios [42, 47]. One proposal is that the DQCP is unreachable (e.g., existing only in space-time dimensionality slightly less than 3), described by a nonunitary conformal field theory [53–58].

In some variants of the  $J$ - $Q$  model, clearly first-order transitions were observed [5, 59, 60]. The "checker-board"  $J$ - $Q$  (CBJQ) model [5] (and a closely related loop model [61]) has a  $\mathbb{Z}_2$  breaking PS phase like that in the SS model. A spin-flop-like transition with emergent  $O(4)$  symmetry of the combined  $O(3)$  AF and scalar PS order parameters was found, with no signs of a conventional coexistence state with tunneling barriers up to the largest length scales studied. This unusual behavior indicates close proximity to an  $O(4)$  DQCP [5, 6].

Lee et al. recently considered a proxy of the excitation gap with the iDMRG method, studying correlation lengths of operators with the symmetries of the excited SS levels of interest [6]. Following Ref. 25, they identified both crossing points discussed here (Figs. 2 and 3), but these points were not extrapolated to infinite size. It was nevertheless argued that the singlet-triplet and singlet-quintuplet crossings will drift to a common DQCP with increasing system size, in the SS model as well as in the  $J_1$ - $J_2$  model. However, in a very recent work, Shackleton et al. revisited the  $J_1$ - $J_2$  model and constructed a

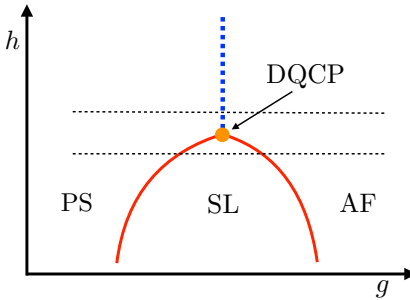


Figure 6. Unified phase diagram, where the DQCP separates a line of first-order PS–AF transitions and an extended SL phase. The PS–SL and SL–AF transition may both be continuous DQCP-like transitions. The dashed horizontal lines illustrate cuts through the phase diagram when a single parameter  $g$  is tuned; corresponding the CBJQ model (top line) and the SS model (bottom line).

quantum field theory of a possible gapless SL phase and a DQCP separating it from the AF state [35].

A narrow SL in the SS model suggests proximity of this phase to the DQCP discussed by Lee et al [6], which then most likely should be the same DQCP as the one influencing the  $O(4)$  transition in the CBJQ model [5]. Moreover, it has recently been argued that the DQCP is actually a multi-critical point [62]; a second relevant scaling field with all the symmetries of the Hamiltonian was detected in the conventional critical  $J$ - $Q$  model. The renormalization-group flow therefore turns toward a first-order transition when a certain interaction is turned on in such a way as to maintain a sign-free path integral [59]. It is possible that the interaction with the opposite sign could instead open up an SL phase. Taken together, all these observations suggest the unified phase diagram schematically illustrated in Fig. 6. The two parameters ( $g, h$ ) correspond to two relevant symmetric fields, and in models with just one tuning parameter, e.g., the CBJQ and SS models, either the first-order line or the SL phase is traversed.

*Summary and Discussion.*—Our DMRG results can consistently be explained by a previously not anticipated SL phase between the known PS and AF phases of the SS model. Our gap scaling results indicate a gapless SL with  $z = 1$ , and for the SL–AF transition we have estimated the anomalous dimension  $\eta \approx 0.20$  for the critical AF order parameter.

The PS–SL point  $g_{c1} \approx 0.79$  is above the PS–AF point  $g_c \approx 0.765$  obtained with tensor product states [14] (where the system is infinite but the results may be affected by small tensors) but is not at significant variance with the more recent iDMRG (infinite-size DMRG, where only  $L_y$  is finite) calculation [6], where  $g_c \approx 0.77$  for  $L = 12$  and an increase in  $g_c$  with  $L$  was observed (see Table 1 of Ref. 6). The tensor technique used in Ref. 14 has a bias to ordered phases, which may force AF order into the fragile SL phase. In Ref. 6 the AF order parameter was not studied, and its appearance only at higher  $g$  (above those reported) may have been missed. While these works did not consider any other phase intervening between the PS and AF phases, an early field theory of the SS model within an  $1/S_i$  expansion (with  $S_i = 1/2$  being the

target spin value) contains phases not detected numerically to date, including a gapped SL but no gapless SL [63].

Given our results and the existence of a gapless SL in the closely related  $J_1$ - $J_2$  model [23, 25, 32–35], such SLs may be ubiquitous between symmetry-breaking singlet and AF phases. It was previously argued that the commonly studied Dirac SLs should be unstable on bipartite lattices and lead to DQCPs [6, 64], and the SL identified here may then fall outside this framework [35]. In our general scenario, in multi-parameter models the SL may be shrunk to a multi-critical DQCP followed by a first-order direct PS–AF transition, which is an alternative to the scenario of an unreachable, non-unitary DQCP [53–58] (though in principle there could also be a triple point instead of the DQCP in Fig. 6).

The DQCP as a point separating a line of first order transitions and an extended SL phase is a compelling scenario also considering that the  $J$ - $Q$  models can be continuously deformed into conventional frustrated models. In the CPJQ model, the  $Q$  terms could reside on the empty SS plaquettes. By gradually turning off the  $Q$  terms and turning on the  $J'$  terms, the unusual first-order PS–AF transition with emergent  $O(4)$  symmetry of the CBJQ model [5] should evolve as if the upper dashed line in Fig. 6 moved down, and eventually the SL phase of the SS model should appear. We plan to study such combined models in the future.

An SL phase in the SS model may explain the absence of any observed phase transition in  $\text{SrCu}_2(\text{BO}_3)_2$  at pressures 2.6 to 3 GPa [7, 8], between the regions where there is strong evidence for PS and AF phases. Since  $\text{SrCu}_2(\text{BO}_3)_2$  samples can be made with very low concentration of impurities, unlike many other potential spin liquid materials, an SL phase would be a very significant development.

*Acknowledgments.*—We would like to thank Frédéric Mila and Subir Sachdev for stimulating discussions, and S.S. also for sending us the preprint Ref. 35. A.W.S. was supported by the Simons Foundation under Simons Investigator Grant No. 511064. L.W. was supported by the National Key Research and Development Program of China, Grant No. 2016YFA0300603, and by the National Natural Science Foundation of China, Grants No. NSFC-11874080 and No. NSFC-11734002. The computational results presented here were achieved partially using Tianhe-2JK computing time awarded by the Beijing Computational Science Research Center (CSRC).

\* sandvik@bu.edu

† lingwangqs@zju.edu.cn

- [1] H. Kageyama, K. Yoshimura, R. Stern, N. V. Mushnikov, K. Onizuka, M. Kato, K. Kosuge, C. P. Slichter, T. Goto, and Y. Ueda, Exact Dimer Ground State and Quantized Magnetization Plateaus in the Two-Dimensional Spin System  $\text{SrCu}_2(\text{BO}_3)_2$ , *Phys. Rev. Lett.* **82**, 3168 (1999).
- [2] S. Miyahara and K. Ueda, Exact Dimer Ground State of the Two Dimensional Heisenberg Spin System  $\text{SrCu}_2(\text{BO}_3)_2$ ,

Phys. Rev. Lett. **82**, 3701 (1999).

[3] A. Koga and N. Kawakami, Quantum Phase Transitions in the Shastry-Sutherland Model for  $\text{SrCu}_2(\text{BO}_3)_2$ , Phys. Rev. Lett. **84**, 4461 (2000).

[4] M. Zayed, Ch. Rüegg, J. Larrea, A. M. Läuchli, C. Panagopoulos, S. S. Saxena, M. Ellerby, D. McMorr, Th. Strässle, S. S. Klotz, G. Hamel, R. A. Sadykov, V. Pomjakushin, M. Boehm, M. Jiménez-Ruiz, A. Schneidewin, E. Pomjakushin, M. Stincaciu, K. Conder, and H. M. Rønnow, 4-spin plaquette singlet state in the Shastry-Sutherland compound  $\text{SrCu}_2(\text{BO}_3)_2$ , Nature Phys. **13**, 962 (2017).

[5] B. Zhao, P. Weinberg, and A. W. Sandvik, Symmetry enhanced first-order phase transition in a two-dimensional quantum magnet, Nature Phys. **15**, 678 (2019).

[6] J. Y. Lee, Y.-Z. You, S. Sachdev, and A. Vishwanath, Signatures of a Deconfined Phase Transition on the Shastry-Sutherland Lattice: Applications to Quantum Critical  $\text{SrCu}_2(\text{BO}_3)_2$ , Phys. Rev. X **9**, 041037 (2019).

[7] J. Guo, G. Sun, B. Zhao, L. Wang, W. Hong, V. A. Sidorov, N. Ma, Q. Wu, S. Li, Z. Y. Meng, A. W. Sandvik, and L. Sun, Quantum Phases of  $\text{SrCu}_2(\text{BO}_3)_2$  from High-Pressure Thermodynamics, Phys. Rev. Lett. **124**, 206602 (2020).

[8] J. Larrea Jiménez, S. P. G. Crone, E. Fogh, M. E. Zayed, R. Lortz, E. Pomjakushina, K. Conder, A. M. Läuchli, L. Weber, S. Wessel, A. Honecker, B. Normand, Ch. Rüegg, P. Corboz, H. M. Rønnow, and F. Mila, A quantum magnetic analogue to the critical point of water, arXiv:2009.14492.

[9] S. Bettler, L. Stoppel, Z. Yan, S. Gvasaliya, and A. Zheludev, Sign switching of dimer correlations in  $\text{SrCu}_2(\text{BO}_3)_2$  under hydrostatic pressure, Phys. Rev. Research **2**, 012010(R) (2020).

[10] T. Senthil, A. Vishwanath, L. Balents, S. Sachdev, and M. P. A. Fisher, Deconfined Quantum Critical Points, Science **303**, 1490 (2004).

[11] S. Sachdev, Quantum magnetism and criticality, Nature Phys. **4**, 173 (2008).

[12] A. W. Sandvik, Evidence for Deconfined Quantum Criticality in a Two-Dimensional Heisenberg Model with Four-Spin Interactions, Phys. Rev. Lett. **98**, 227202 (2007).

[13] B. S. Shastry and B. Sutherland, Exact ground state of a quantum mechanical antiferromagnet, Physica B+C **108**, 1069 (1981).

[14] P. Corboz and F. Mila, Tensor network study of the Shastry-Sutherland model in zero magnetic field, Phys. Rev. B **87**, 115144 (2013).

[15] H. Nakano and T. Sakai, Third Boundary of the Shastry-Sutherland Model by Numerical Diagonalization, J. Phys. Soc. Jpn. **87**, 123702 (2018).

[16] T. Waki, K. Arai, M. Takigawa, Y. Saiga, Y. Uwatoko, H. Kageyama, and Y. Ueda, A novel ordered phase in  $\text{SrCu}_2(\text{BO}_3)_2$  under high pressure, J. Phys. Soc. Jpn. **76**, 073710 (2007).

[17] C. Boos, S. P. G. Crone, I. A. Niesen, P. Corboz, K. P. Schmidt, and F. Mila, Competition between intermediate plaquette phases in  $\text{SrCu}_2(\text{BO}_3)_2$  under pressure, Phys. Rev. B **100**, 140413 (2019).

[18] G. Sun, N. Ma, B. Zhao, A. W. Sandvik, and Z. Y. Meng, Emergent  $O(4)$  symmetry at the phase transition from plaquette-singlet to antiferromagnetic order in quasi-two-dimensional quantum magnets, arXiv:2103.00863 (to appear in Chin. Phys. B).

[19] S.R. White, Density Matrix Formulation for Quantum Renormalization Groups, Phys. Rev. Lett. **69**, 2863 (1992).

[20] U. Schollwöck, The density-matrix renormalization group in the age of matrix product states, Ann. Phys. (Amsterdam) 326, **96** (2011).

[21] E. M. Stoudenmire and S. R. White, Real-space parallel density matrix renormalization group, Phys. Rev. B **87**, 155137 (2013).

[22] A. Weichselbaum, Non-abelian symmetries in tensor networks: A quantum symmetry space approach, Ann. Phys. (Amsterdam) **327**, 2972 (2012).

[23] S.-S. Gong, W. Zhu, D. N. Sheng, O. I. Motrunich, and M. P. A. Fisher, Plaquette Ordered Phase and Quantum Phase Diagram in the Spin-1/2  $J_1$ - $J_2$  Square Heisenberg Model, Phys. Rev. Lett. **113**, 027201 (2014).

[24] I. P. McCulloch, From density-matrix renormalization group to matrix product states, J. Stat. Mech. (2007) P10014.

[25] L. Wang and A. W. Sandvik, Critical Level Crossings and Gapless Spin Liquid in the Square-Lattice Spin-1/2  $J_1$ - $J_2$  Heisenberg Antiferromagnet, Phys. Rev. Lett. **121**, 107202 (2018).

[26] M. Lemm, A. W. Sandvik, and L. Wang, Existence of a Spectral Gap in the Affleck-Kennedy-Lieb-Tasaki Model on the Hexagonal Lattice, Phys. Rev. Lett. **124**, 177204 (2020).

[27] See Supplemental material for additional discussion of the DMRG convergence procedures and the 2D real-space landscape of PS ordering.

[28] K. Nomura and K. Okamoto, Fluid-dimer critical point in  $S = 1/2$  antiferromagnetic Heisenberg chain with next nearest neighbor interactions, Phys. Lett. A **169**, 433 (1992).

[29] S. Eggert, Numerical evidence for multiplicative logarithmic corrections from marginal operators, Phys. Rev. B **54**, R9612 (1996).

[30] A. W. Sandvik, Ground States of a Frustrated Quantum Spin Chain with Long-Range Interactions, Phys. Rev. Lett. **104**, 137204 (2010).

[31] H. Suwa, A. Sen, and A. W. Sandvik, Level spectroscopy in a two-dimensional quantum magnet: Linearly dispersing spinons at the deconfined quantum critical point, Phys. Rev. B **94**, 144416 (2016).

[32] Y. Nomura and M. Imada, Dirac-type nodal spin liquid revealed by machine learning, arXiv:2005.14142.

[33] F. Ferrari and F. Becca, Gapless spin liquid and valence-bond solid in the  $J_1$ - $J_2$  Heisenberg model on the square lattice: Insights from singlet and triplet excitations, Phys. Rev. B **102**, 014417 (2020).

[34] S. Morita, R. Kaneko, and M. Imada, Quantum spin liquid in spin 1/2  $J_1$ - $J_2$  Heisenberg model on square lattice: Many-variable variational Monte Carlo study combined with quantum-number projections, J. Phys. Soc. Jpn. **84**, 024720 (2015).

[35] H. Shackleton, A. Thomson, and S. Sachdev, Deconfined criticality and a gapless  $\mathbb{Z}_2$  spin liquid in the square lattice antiferromagnet (unpublished).

[36] B. Zhao, J. Takahashi, and A. W. Sandvik, Comment on “Gapless spin liquid ground state of the spin-1  $J_1$ - $J_2$  Heisenberg model on square lattices”, Phys. Rev. B **101**, 157101 (2020).

[37] R. G. Melko and R. K. Kaul, Scaling in the Fan of an Unconventional Quantum Critical Point, Phys. Rev. Lett. **100**, 017203 (2008).

[38] F.-J. Jiang, M. Nyfeler, S. Chandrasekharan, and U.-J. Wiese, From an antiferromagnet to a valence bond solid: evidence for a first-order phase transition, J. Stat. Mech.: Theory Exp. **2008**, P02009 (2008).

[39] J. Lou, A. W. Sandvik, and N. Kawashima, Antiferromagnetic to valence-bond-solid transitions in two-dimensional  $SU(N)$  Heisenberg models with multispin interactions, Phys. Rev. B **80**, 180414 (R) (2009).

[40] A. W. Sandvik, Continuous Quantum Phase Transition between an Antiferromagnet and a Valence-Bond Solid in Two Dimen-

sions: Evidence for Logarithmic Corrections to Scaling, *Phys. Rev. Lett.* **104**, 177201 (2010).

[41] R. K. Kaul, Quantum criticality in SU(3) and SU(4) antiferromagnets, *Phys. Rev. B* **84**, 054407 (2011).

[42] A. W. Sandvik, Finite-size scaling and boundary effects in two-dimensional valence-bond solids, *Phys. Rev. B* **85**, 134407 (2012).

[43] M. S. Block, R. G. Melko, and R. K. Kaul, Fate of  $\mathbb{CP}^{N-1}$  Fixed Points with  $q$  Monopoles, *Phys. Rev. Lett.* **111**, 137202 (2013).

[44] K. Harada, T. Suzuki, T. Okubo, H. Matsuo, J. Lou, H. Watanabe, S. Todo, and N. Kawashima, Possibility of deconfined criticality in SU(N) Heisenberg models at small N, *Phys. Rev. B* **88**, 220408(R) (2013).

[45] K. Chen, Y. Huang, Y. Deng, A. B. Kuklov, N. V. Prokof'ev, and B. V. Svistunov, Deconfined Criticality Flow in the Heisenberg Model with Ring-Exchange Interactions, *Phys. Rev. Lett.* **110**, 185701 (2013).

[46] S. Pujari, F. Alet, and K. Damle, Transitions to valence-bond solid order in a honeycomb lattice antiferromagnet, *Phys. Rev. B* **91**, 104411 (2015).

[47] H. Shao, W. Guo, A. W. Sandvik, Quantum criticality with two length scales, *Science* **352**, 213 (2016).

[48] A. W. Sandvik and B. Zhao, Consistent scaling exponents at the deconfined quantum-critical point, *Chin. Phys. Lett.* **37**, 057502 (2020).

[49] A. Nahum, P. Serna, J. T. Chalker, M. Ortúñ, and A. M. Somoza, Emergent SO(5) Symmetry at the Néel to Valence-Bond-Solid Transition, *Phys. Rev. Lett.* **115**, 267203 (2015).

[50] A. Nahum, J. T. Chalker, P. Serna, M. Ortúñ, and A. M. Somoza, Deconfined Quantum Criticality, Scaling Violations, and Classical Loop Models, *Phys. Rev. X* **5**, 041048 (2015).

[51] G. Sreejith, S. Powell, and A. Nahum, Emergent SO(5) symmetry at the columnar ordering transition in the classical cubic dimer model, *Phys. Rev. Lett.* **122**, 080601 (2019).

[52] Z. Wang, M. P. Zaletel, R. S. K. Mong, and F. F. Assaad, Phases of the (2+1) dimensional SO(5) non-linear sigma model with topological term, *Phys. Rev. Lett.* **126**, 045701 (2021).

[53] C. Wang, A. Nahum, M. A. Metlitski, C. Xu, and T. Senthil, Deconfined Quantum Critical Points: Symmetries and Dualities, *Phys. Rev. X* **7**, 031051 (2017).

[54] V. Gorbenko, S. Rychkov, and B. Zan, Walking, weak first-order transitions, and complex CFTs, *J. High Energy Phys.* **2018**, 108 (2018).

[55] V. Gorbenko, S. Rychkov, and B. Zan, Walking, Weak first-order transitions, and Complex CFTs II. Two-dimensional Potts model at  $Q > 4$ , *SciPost Phys.* **5**, 050 (2018).

[56] R. Ma and C. Wang, A theory of deconfined pseudo-criticality, *Phys. Rev. B* **102**, 020407 (2020).

[57] A. Nahum, Note on Wess-Zumino-Witten models and quasi-universality in 2+1 dimensions, *Phys. Rev. B* **102**, 201116(R) (2020).

[58] Y.-C. He, J. Rong, and N. Su, Non-Wilson-Fisher kinks of  $O(N)$  numerical bootstrap: from the deconfined phase transition to a putative new family of CFTs, *arXiv:2005.04250*.

[59] B. Zhao, J. Takahashi, and A. W. Sandvik, Tunable deconfined quantum criticality and interplay of different valence-bond solid phases, *Chin. Phys. B* **29**, 057506 (2020).

[60] J. Takahashi and A. W. Sandvik, Valence-bond solids, vestigial order, and emergent  $SO(5)$  symmetry in a two-dimensional quantum magnet, *Phys. Rev. Research* **2**, 033459 (2020).

[61] P. Serna and A. Nahum, Emergence and spontaneous breaking of approximate  $O(4)$  symmetry at a weakly first-order deconfined phase transition, *Phys. Rev. B* **99**, 195110 (2019).

[62] B. Zhao, J. Takahashi, and A. W. Sandvik, Multicritical Deconfined Quantum Criticality and Lifshitz Point of a Helical Valence-Bond Phase, *Phys. Rev. Lett.* **125**, 257204 (2020).

[63] C. H. Chung, J. B. Marston, and S. Sachdev, Quantum phases of the Shastry-Sutherland antiferromagnet: Application to  $SrCu_2(BO_3)_2$ , *Phys. Rev. B* **64**, 134407 (2001).

[64] X.-Y. Song, Y.-C. He, A. Vishwanath, and C. Wang, From Spinon Band Topology to the Symmetry Quantum Numbers of Monopoles in Dirac Spin Liquids, *Phys. Rev. X* **10**, 011033 (2020).

## Supplemental Material

### Quantum Criticality and Spin Liquid Phase in the Shastry-Sutherland model

Jianwei Yang,<sup>1</sup>, Anders W. Sandvik,<sup>2,3,\*</sup>, Ling Wang<sup>4,†</sup>

<sup>1</sup> *Beijing Computational Science Research Center, 10 East Xibeiwang Road, Beijing 100193, China*

<sup>2</sup> *Department of Physics, Boston University, 590 Commonwealth Avenue, Boston, Massachusetts 02215, USA*

<sup>3</sup> *Beijing National Laboratory for Condensed Matter Physics*

*and Institute of Physics, Chinese Academy of Sciences, Beijing 100190, China*

<sup>4</sup> *Department of Physics, Zhejiang University, Hangzhou 310000, China*

\* e-mail: sandvik@bu.edu, † lingwangqs@zju.edu.cn

Here we present additional results in support of the conclusions drawn in the main paper. In Sec. 1 we discuss the DMRG procedures used and illustrate the convergence properties and extrapolations of energies and order parameters. In Sec. 2 we present 2D plots of the PS order 'landscape' and discuss the effects of the open  $x$  boundaries of the cylindrical lattices, including an explanation for the non-monotonic behavior of the PS order parameter for  $g \geq 0.80$  in Fig. 5.

#### 1. DMRG convergence and extrapolations

In order to systematically approach the correct ground states and excitations in the DMRG calculations, we carry out calculations for several numbers  $m$  of Schmidt states, until either  $m$  is sufficiently large for the discarded weight  $\epsilon$  to be negligible (in case of the smaller system sizes considered here) or sufficiently small for reliably extrapolating to  $\epsilon = 0$  (for the largest system sizes). The discarded weight is defined in the standard way as the sum of discarded eigenvalues of the reduced density matrix [20, 21]. After an initial calculation for small  $m$ , each subsequent calculation is started from a previously well converged calculation for a smaller  $m$ . For a given  $m$ , we demand that the energy difference (not divided by the system volume) between two successive updating sweeps is less than  $10^{-6}$ . We then check the convergence of the energies and other quantities as a function of the discarded weight  $\epsilon$  (which depends on  $m$ , with  $\epsilon \rightarrow 0$  as  $m \rightarrow \infty$ ).

Our DMRG program is implemented with full SU(2) symmetry [22, 23], and we can therefore target the ground state of any sector of total spin  $S$ . Given that the lowest ground state among these has  $S = 0$  and we are also interested in the lowest  $S = 0$  excitation, in this sector we apply the technique of orthogonalizing to the previously calculated ground state in order to target the lowest excited  $S = 0$  state [24–26].

In Fig. S1 we show the lowest two  $S = 0$  energies as well as the  $S = 1$  energy for system sizes  $L = 6, 8, 10$ , and 12, in the important case of  $g = 0.80$  (inside the new gapless SL phase). For the challenging  $L = 12$  system, we used  $m$  up to 8000 for the  $S = 0$  ground state and up to  $m = 9000$  for the excited singlet. We do not have sufficiently good  $S = 1$  results for  $L = 12$  and therefore only show  $S = 1$  results for the smaller systems in Fig. S1.

For  $L = 6$ , the calculation for the largest  $m$  already has

an extremely small discarded weight and it is not necessary to further extrapolate the results. We nevertheless show extrapolations for all system sizes. While the exact form of the error as a function of  $\epsilon$  in the DMRG method is not known, in all cases for which data are presented in the main paper our results are sufficiently converged for the extrapolated values to not be very sensitive to the fitting form used. We have found that the energies for small  $\epsilon$  are well described by third-order polynomials without linear term. Thus, in Fig. S1 all data are fitted to such a form.

In the case of the order parameters, we find that polynomial fits work well in general (here including the linear terms). We typically use third-order forms. Examples for the two largest system sizes,  $L = 12$  and  $L = 14$  for  $g = 0.8$ , are shown in Fig. S2. Here the  $L = 14$  data for  $m_s^2$  are not yet quite in the regime where a generic polynomial extrapolation produces stable results with respect to the polynomial order and the number of points included in the fit. An unconstrained polynomial fit typically leads to a slightly non-monotonic form. Given that we have seen no signs of non-monotonic convergence behaviors in other cases (where generic polynomial fits are stable), we therefore have constrained the polynomial to produce a monotonic form also in this  $L = 14$  case (but not for smaller lattices). Depending on exactly what form is used and how many data points are included, there are some variations in the extrapolated  $\epsilon = 0$  value for  $m_s^2$ . However, it should be noted that the overall range of the  $y$ -axis of Fig. S2(c) represents a very small relative change in the value, and the uncertainties in the extrapolation for this case (less than 0.3% between different extrapolations, including non-monotonic cases) do not impact the conclusions drawn on the basis of the data in Fig. 5.

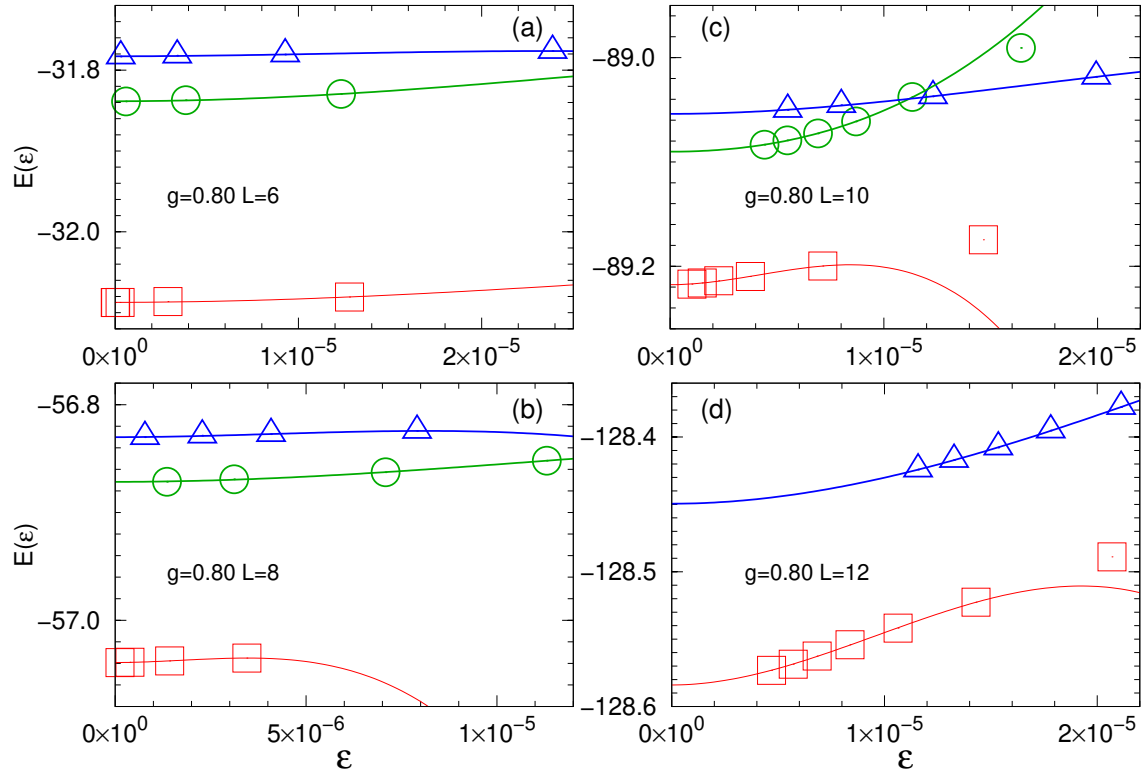


Figure S1. Examples of extrapolations of DMRG energies to vanishing discarded weight  $\epsilon$  for the SS model with  $g = 0.8$ . For each of the system sizes  $L = 6, 8, 10, 12$  in panels (a)-(d), the two lowest singlets are shown (squares and triangles) along with the lowest triplet (circles), except for  $L = 12$ , for which we do not have sufficiently well converged triplet data. The fitted curves are of the form  $E(\epsilon) = E(0) + a\epsilon^2 + b\epsilon^3$ , with  $E(0)$ ,  $a$ , and  $b$  optimized parameters.

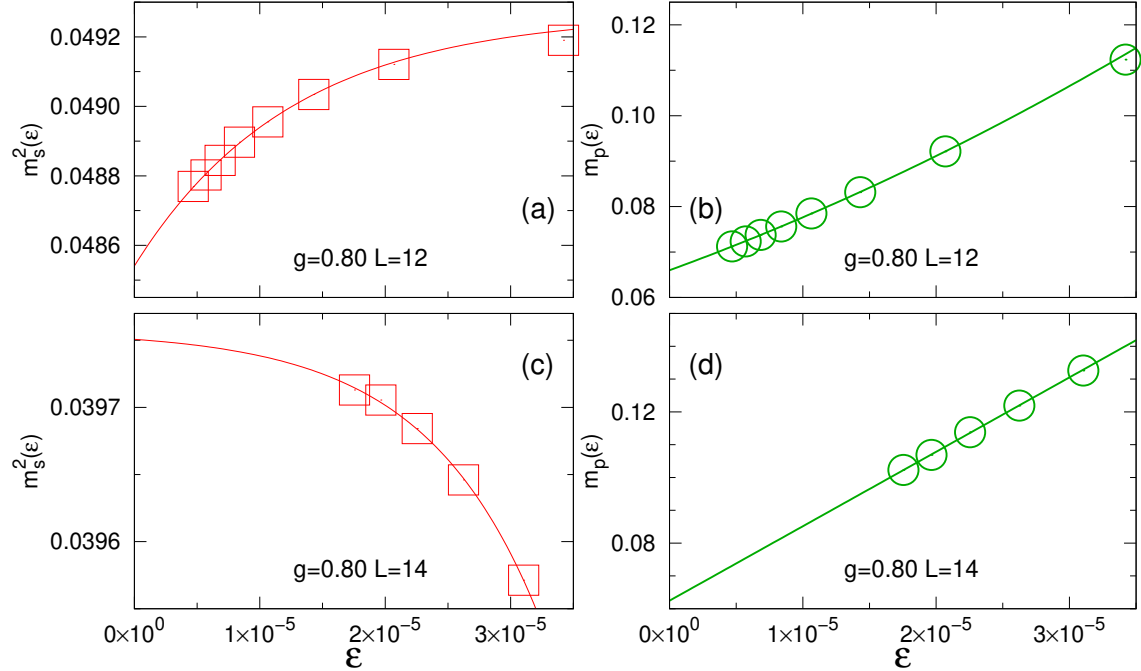


Figure S2. Examples of extrapolations of DMRG results for the AF and PS order parameters in the ground state of the SS model at  $g = 0.8$ . Results for system size  $L = 12$  are shown in (a) and (b), and corresponding results for  $L = 14$  are shown in (c) and (d). The fitting forms for  $L = 12$  are third-order polynomials. For  $L = 14$  a second-order polynomial is used for  $m_p$  in (d), while a fourth-order polynomial with only even powers is used for  $m_s^2$  in (c) to ensure a monotonic form.

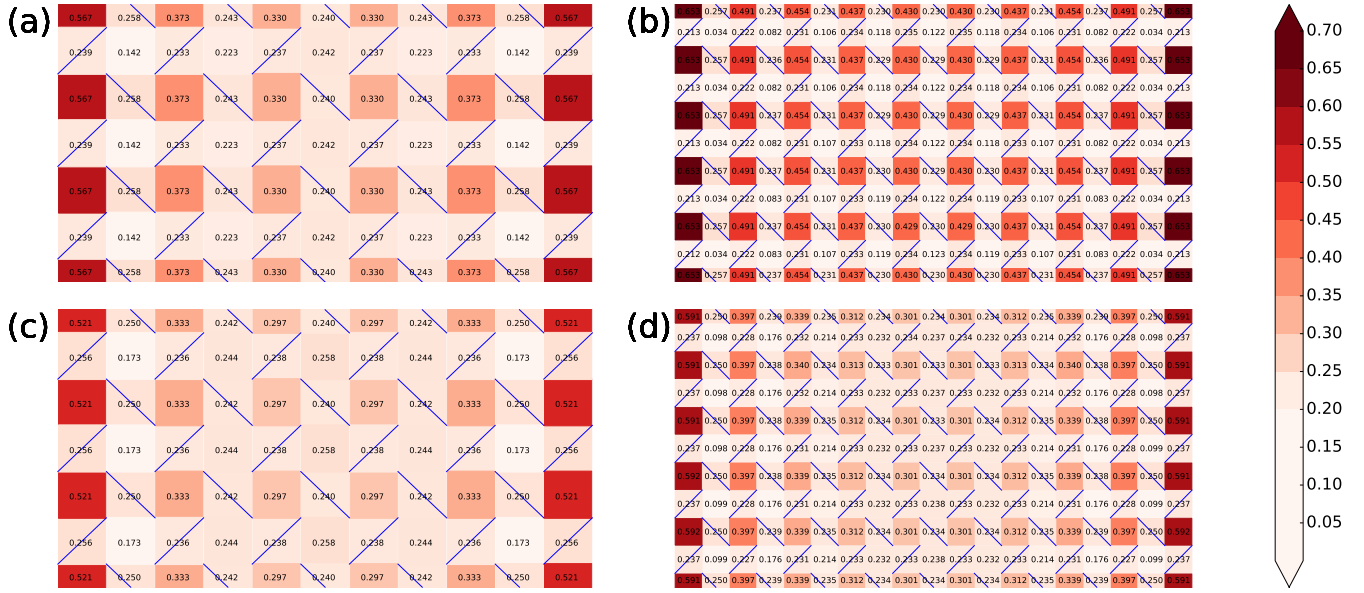


Figure S3. Landscape of plaquette singlet strengths in systems of size  $L = 6$  (left) and  $L = 10$  (right), for  $g = 0.75$  (inside the PS phase) in (a) and (b), and for  $g = 0.80$  (in the SL phase) in (c) and (d). The colored squares correspond to the expectation value  $\langle Q_R \rangle$  of the plaquette operator defined in the main paper for the plaquettes at lattice coordinate  $\mathbf{R}$ . The SS dimer couplings  $J'$  are indicated with the blue lines. In addition to the color coding shown on the vertical bar, the actual numerical values of  $\langle Q_R \rangle$  are also displayed inside each square.

## 2. Role of cylinder edges

As shown in Fig. 1 in the main paper, the PS ordering pattern is unique on the cylindrical lattices used here. The cylinder edges act as a  $\mathbb{Z}_2$  symmetry-breaking field, allowing us to study the PS order parameter  $m_p$  directly, instead of using the squared order parameter in a system with unbroken symmetry. This approach was discussed in detail in Ref. 36 in the context of a different system, and it was argued that it is the best way to study the order parameters of 'singletized' phases with methods that use symmetry-breaking boundary conditions.

Fig. S3 shows examples of the singlet pattern forming on two different lattices sizes,  $L = 6$  and  $L = 10$ , both inside the PS phase at  $g = 0.75$  and in the SL phase at  $g = 0.80$ . In the PS phase, we can observe that the alternating pattern of strong and weak empty plaquettes (those without the SS diagonal couplings  $J'$ ) is much stronger in the larger systems. This order enhancement with increasing  $L$  in the PS phase was already seen in the size dependent  $m_p$ , defined as the difference between central adjacent empty plaquettes, in the inset of Fig. 5 in the main paper. The strengthening of the PS order clearly reflects the diminishing quantum fluctuations with increasing system size in the presence of the symmetry-breaking edge field. Note that the edge order also strengthens with increasing  $L$ .

Turning now to the results in the SL phase, Fig. S3(c) and S3(d), here as well we observe how the edge order is significantly stronger in the larger system. The bulk order parameter, defined in the center of the system, is also stronger in the larger system. However, as seen in the inset of Fig. 5 in the main paper, for the largest system size considered for  $g = 0.80$ ,  $L = 14$ ,  $m_p$  has turned downward. This non-monotonic behavior outside the PS phase can naturally be explained as a competition between the always present (for any  $g$ ) symmetry breaking at the cylinder edge and the decay of this 'artificial' order in the central part of the system as  $L$  increases. The initial increase with  $L$  for small systems is due to the strengthening of the edge order with  $L$  even when the system is in the SL or AF phase. The eventual down-turn of the order parameter for larger systems is a sign of this edge effect not extending to the bulk, i.e., that the system is not in the PS phase.

It is difficult to imagine any realistic mechanism that would cause  $m_p$  to turn back up as  $L$  increases further after the peak value has been reached and  $m_p$  has begun to decrease with  $L$ . Therefore, we regard the observation of a maximum in  $m_p$  for a given  $L$  as a definite indicator of the system not being in the PS phase. Our results for  $g = 0.80-0.84$  in Fig. 5 all exemplify this behavior.